We are IntechOpen, the world's leading publisher of Open Access books Built by scientists, for scientists

4,800
Open access books available

122,000
International authors and editors

135M
Downloads

Our authors are among the

154
Countries delivered to

TOP 1%
most cited scientists

12.2%
Contributors from top 500 universities

CLARIVATE ANALYTICS BOOK CITATION INDEX INDEXED

WEB OF SCIENCE™

Selection of our books indexed in the Book Citation Index in Web of Science™ Core Collection (BKCI)

Interested in publishing with us?
Contact book.department@intechopen.com

Numbers displayed above are based on latest data collected.
For more information visit www.intechopen.com

Chapter 1

Pulsed Electric Current Sintering of Transparent Alumina Ceramics

Makoto Nanko and Khanh Quoc Dang

Additional information is available at the end of the chapter

http://dx.doi.org/10.5772/59170

1. Introduction

Aluminum oxide (Al_2O_3) commonly referred as to alumina is one of the most widely used as engineering oxide ceramics. From crystalline structure difference, there are many forms of Al_2O_3 (α, χ, η, δ, θ, γ and ϱ), with α-Al_2O_3 being thermodynamically the most stable form. An example of α phase of Al_2O_3 is corundum or sapphire [1]. In the present chapter, α-Al_2O_3 is discussed and described as Al_2O_3. With a high melting temperature, chemical stability, Al_2O_3 is leading to applications as high-temperature components, catalyst substrates and biomedical implants. Al_2O_3 has excellent optical transparency and along with additives such as chromium and titanium, it is important as a sodium lamp (sapphire), a gem stone (sapphire and ruby) and a laser host (ruby).

Usually, Al_2O_3 ceramics were produced by sintering Al_2O_3 powder, that is, polycrystalline Al_2O_3. Sintered polycrystalline Al_2O_3 ceramics were opaque because of light scattering by closed pores and grain boundaries. In order to fabricate transparent polycrystalline Al_2O_3, many sintering techniques have been studied such as hot-pressing (HP), hot isostatic pressing (HIP), microwave sintering and pulsed electric current sintering (PECS).

PECS is also known as spark plasma sintering (SPS) or plasma activated sintering (PAS). The sintering technique is the latest pressure-sintering process to consolidate advanced materials such as ceramics, metallic materials, composites, polymers, semiconductors and oxide superconductors, in which the powder is heated by the application of electric current under uniaxial pressure.

PECS is a promising sintering technique for producing transparent polycrystalline Al_2O_3. In the present chapter, progress in PECS for transparent Al_2O_3 was discussed as well as other

oxides. Fundamentals of PECS were also discussed in the present chapter in order to understand PECS for transparent Al_2O_3.

2. Fundamentals on PECS

According to the open literatures [2, 3], the electric current activated/assisted sintering technology was pioneered by Duval d'Adrian in 1922 [4]. However, the first patent on pure direct current (DC) resistance sintering (RS) was proclaimed by Bloxam in 1906 [5, 6]. Thereafter, Taylor [7-9] developed the resistive sintering process consisting of capacitors, transformers and special switching devices. This process originated the electric discharge compaction (EDC) [10].

Inoue [11, 12] developed the first concept of the PECS technology in 1966. It introduced different electric current waveforms, i.e. low-frequency alternate current (AC), high-frequency unidirectional AC or pulsed DC. These sintering techniques were combined in one sintering process of electric-discharge sintering (EDS) [11], also known as spark sintering (SS). In SS process, a unidirectional pulsed DC or a unidirectional AC, is applied, then DC is eventually superimposed. This process led the development of current PECS technology, e.g. plasma activated sintering (PAS), spark plasma sintering (SPS), filed assisted sintering and plasma pressure compaction® (P^2C) [13].

In the late 1980s various companies started to manufacture PECS machines based on Inoue's patents. Since then, the number of the PECS applications has been extended further. In the early 1990s, Sumitomo Coal Mining Co. commercialized the new PECS apparatuses (2-20 kA DC pulse generators, 98-980 kN load cells) [14, 15]. The PECS process is schematically shown in Figure 1.

It simultaneously applies an electric current along with a uniaxial pressure in order to accelerate densification of powders with desired configuration [16]. The electric current delivered during PECS processes could in general assume different intensity and waveform which depend upon the power supply characteristics [2, 3, 14, 16].

The PECS process is characterized by the application of the pulsed electric current during sintering. The heating rate in the PECS process depends on the materials and shapes of the die/sample ensemble and on the electric power supply. Heating rates from 100 to 600 K/min can be obtained in the current PECS equipments. As a consequence, the PECS process can be in time ranges from a few ten seconds to minutes depending on the material and its size to be sintered, configuration and equipment capacity.

The temperature is measured either with a pyrometer focused on the surface of the graphite die or with the thermocouple inserted into the die. Usually, the measured temperature at the surface of the die (die temperature) is lower than that of the sample (sample temperature). The magnitude of this temperature difference depends on a number of factors such as thermal conductivity of the die and the sample, the heating rate used, the pressure used, how well the die is thermal insulated etc. [17]. The current and consequent temperature distributions within

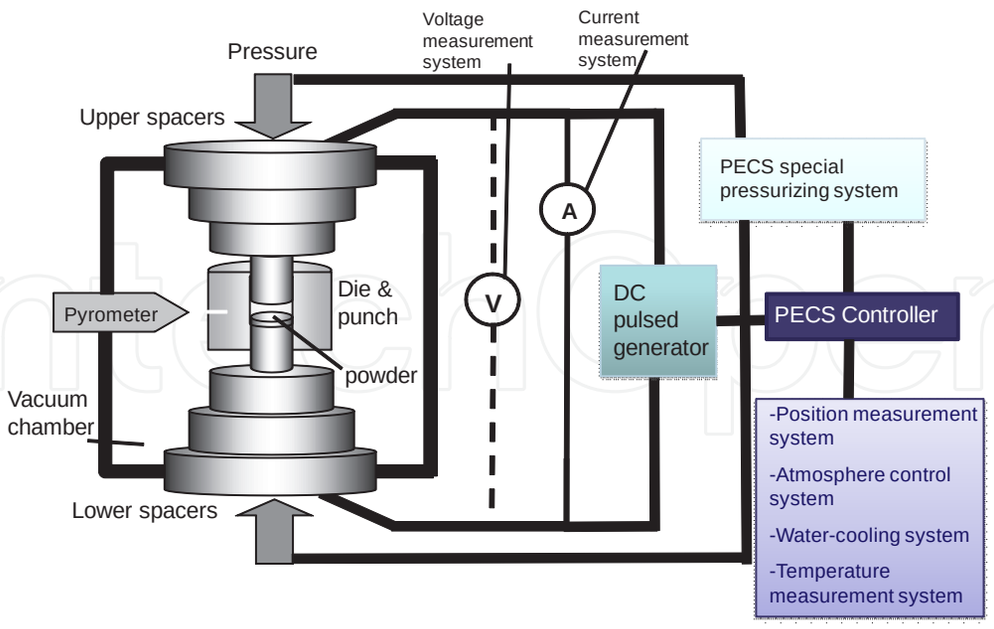

Figure 1. Schematic representation of the PECS process

the sample inside are very important to the homogeneity of density and grain size distribution of the product. Locally dense parts, at the beginning of current flow in particular, may result in locally overheating or even melting [16]. Experimental evidence of temperature distributions with different conductivity materials have been reported in [18-24]. It has been verified that the electrical properties of the sample influence significantly the temperature distributions inside the die as well as sample inside. Thus, in a nonconductive sample (i.e. Si_3N_4 and Al_2O_3), larger thermal gradients has been sometimes observed than in the case of a conductive one (i.e. Ti and Ni), indicating that the temperature distribution within the nonconductive sample is not as homogeneous as within a conductive sample.

Current understanding of the effects of pulse current waveform on compact density in a PECS process is still incomplete. The pulse current did not affect significantly the PECS of cast-iron powder [20] and Ni-20Cr powder [21]. In the PECS process of Al powder, densification behavior is independent of pulse frequency ranging from 300 Hz to 20 kHz [25]. The applied current, however, can significantly affect the growth of the product layer in chemical reaction between Mo and Si plates [26, 27]. With the PECS process, the pulse DC current affected the growth of Nb-C system, Mo_2C layer formed in Mo/C, Ti/C and Zr/C diffusion couples [28-30]. Inoue claimed that there was a frequency-dependent effect in his patent [31]. The densification rate of Fe and Ni based alloy processed by pulsed current was about 5% faster than by direct current [32].

However, the sintering mechanism of insulating oxides such as Al_2O_3 using the PECS method is still an on-going research area. Many papers on PECS of Al_2O_3 powder focused on densification and grain growth behavior by investigating effects of various parameters such as particle size, heating rate, sintering time, pressure and sintering temperature during the PECS

process. Influences of the sintering parameters on densification and grain growth are not clear yet.

There are no reports about pulse current waveform effects on sintering behavior of Al_2O_3. The waveform of applied current is probably an important factor to the sintering process of Al_2O_3. An effect of two types of pulse current waveforms, inverter and pulsed DC, on sample temperature and densification of Al_2O_3 powder by using the PECS process has been clarified in [33-35]. The magnitude of the voltage peaks increased with an increase of the "OFF" time relative to the "ON" time for all of pulse power generator. Maximum voltage value of the inverter generator was higher than that of the pulsed DC generator. PECS with the inverter generator had higher sample temperature than that with the pulsed DC generator.

In PECS of Al_2O_3 powder, the electric current would be mostly applied to the punches and graphite die for heating up to sintering temperature. The average peak height of the 12/2 pulsed DC pattern is lower than that of the 2/6 pulsed DC pattern as well as lower than that of 40/10 inverter and 10/20 inverter pattern at the same die temperature. The inverter-type PECS had a higher voltage applied to the graphite die than the pulsed DC-type ones at the same die temperature. When the number of the "OFF" pulses increased as in the 10/20 inverter or the 2/6 pulsed DC pattern, the peak height of voltages of the "ON" pulses must have increased to keep the output power constant.

Temperature difference in Al_2O_3 sample is generated in PECS [33-35]. When PECS of Al_2O_3 sample with ϕ15 in diameter and 3 mm in thickness was conducted, temperature of sample outside was 20 - 30 K higher than that of the inside sample. The difference of inside/outside temperature using pulsed DC was approximately 10 K lower compared to the inside/outside temperature using the inverter. PECS with an inverter had a higher sample temperature than that with a pulsed DC power generator and it also higher than the die temperature. When the die temperature is increased, the temperature difference between the die surface and the sample also increases.

The sample temperature would be strongly affected by the applied current profile during the PECS process. The current flow should be strongly dependent on the characteristics of the different elements which compose the system (powder, punches, die) and, particularly, their electrical and thermal characteristics. For an insulating material, the applied current does not flow through the sample when a pulse current power is applied to the die-sample, but could only flow from one punch to the other punch via the die. The current forms a magnetic field in the near surface of punches and the die inside where is close to the sample surface, and this magnetic field affects current density [19, 33-37]. The highest current density should be located close to the sample surface as can be illustrated in Figure 2. The temperature distribution is closely related to the current distribution because the heat transfer is generated by the flow of current at the graphite die and the punches. Thus, during the PECS process, the Al_2O_3 powder must be sintered by the heat transferred from the die inside close to the sample surface and punches by means of heat conduction. Given that heat generation and transfer lead to a temperature distribution, temperature outside is higher than that inside the sample [33-35]. In the punch-compression direction, the die temperature is lower than the sample because the

punches are in contact with water-cooled jacket and the die is cooled by radiation from the die outer surface.

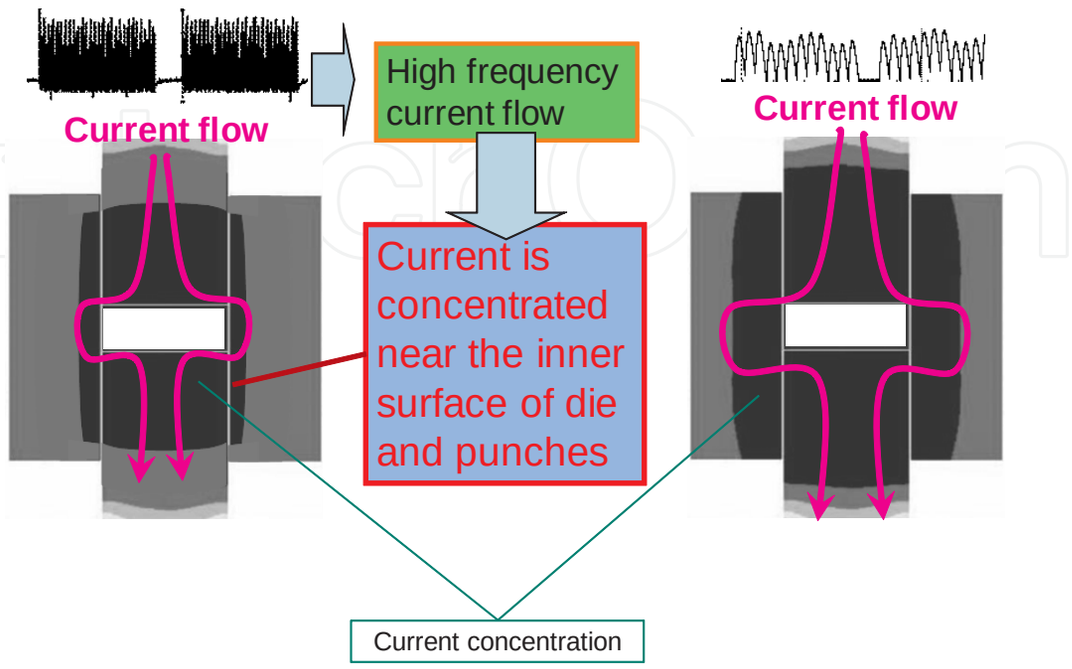

Figure 2. Current flows and distributions in the PECS die/punch/sample system for various pulse waveforms.

The ON/OFF pulse patterns and power generator frequency could also affect the sample temperature. In the case of inverter power waveform, high voltage with high frequency at long "OFF" time flows into die and punch gives higher heat transfer to heat sample than that of other pulse patterns. The difference in sample temperature using pulse current waveform inverter and pulsed DC could be explained by the skin effect as shown in Figure 2. In the punch/die/sample system, the back color area shows the current concentration during the PECS process. In both cases, the heat is generated only in the conductive die and the distribution of the heat generation does not change drastically with the electric conductivity of sample. Electric current distribution is the main cause of the temperature gradient between the sample and the external surface of the die, together with radiation heat from the die surface. When the high frequency current (inverter generator) is applied to punches and graphite die, the current density near the inner surface of the punches/die should be higher than that at its center. In contrast, at low frequency (pulsed DC generator), current density would be uniformly distributed across graphite die and punches. This difference suggests that higher temperature could be achieved due to higher applied voltages, and the required energy for heating a sample with an inverter is higher than that with pulsed DC generator [19, 33-37]. The relative density as a function of the outside/inside sample temperature was discussed in [33-37]. These results show a consistent relative density increase trend with an increase in the sample temperature, independent of the applied pulse current waveforms and ON/OFF patterns. It was also revealed that the average grain size increases with an increase in sample temperature even in different pulse current waveforms and ON/OFF patterns. Densification and grain growth were

predominated by sample temperature. The pulse electric current waveform had effects on the sample temperature, but did not have direct influence on the densification, grain growth and homogeneity of the sample sintered by the PECS process.

3. Sintering of transparent polycrystalline alumina

Transparent polycrystalline Al_2O_3 has increasingly become the focus of recent investigations primarily because of their unique combination of properties. Single crystals of Al_2O_3 are highly transparent in visible and IR region. However polycrystalline Al_2O_3 ceramics are usually opaque because of light scattering of pores and grain boundaries as well as impurities. High density is the most important factor to produce polycrystalline transparent ceramics, as well as grain size. Because of the high efficiency of pores for light scattering, transparency in polycrystalline materials requires extremely low level in porosity, less than 0.01 vol.%. Samples with such low porosity could only be produced under proper sintering conditions involving high temperatures and long sintering time. Residual porosity is much more important than grain boundaries for obtaining the transparency, even in crystallographically anisotropic materials in optical properties. The scattering efficiency for spherical pores, however, decreases dramatically when the pore size in the nanometric range could be achieved [38-40]. It is believed that nanostructured polycrystalline materials would possess higher transparency than ones with the micrometric grain size range. The sintering process at high temperature causes extensive grain growth and then seriously degrades the mechanical properties of the material. What is more important, the higher/bigger grain size larger than 410 μm leads to significant light scattering coming from the birefringence of coarse Al_2O_3 grains [41].

After Coble developed transparent polycrystalline Al_2O_3 [42], many studies for producing transparent polycrystalline Al_2O_3 by sintering techniques were reported [40, 41, 43-82]. Recently, fine-grained transparent polycrystalline Al_2O_3 has attracted much attention due to its superior mechanical and optical properties. This material is prepared by sintering using HP and HIP at low temperature ranging from 1150 to 1400°C. The formation of nanostructure (< 1 μm) results in a significant improvement in both the mechanical strength and the optical transparency. It is reported that the mechanical strength of the fine-grained transparent Al_2O_3 is reached up to 400 - 600 MPa together with a high in-line transmission up to 60 % for visible light [41, 45]. Thus far, the addition of small amount of MgO is known to suppress normal and abnormal grain growth. The MgO concentration needed to inhibit abnormal grain growth depends on other impurities, CaO, SiO_2 etc.. [42, 46, 47, 70, 72]. Coble opened a new chapter that positive effect of 250 ppm MgO addition in sintering of Al_2O_3 is accompanied by dissolution into Al_2O_3 and excess MgO beyond its solid solubility limit exists as non-stoichiometric $MgAl_2O_4$ spinel at the grain boundaries of Al_2O_3 [42]. Hence, MgO strongly segregates into Al_2O_3 grain boundaries and produces a solute drag effect. The resultant microstructure is finer in grain size with higher final density. The transparent MgO doped Al_2O_3 ceramics was sintered to full density and had an in-line transmission of 40-50 % between 400 and 600 nm of the wavelength.

On the other hand, HPed Al_2O_3 yielding better transparency than pressureless-sintered samples was reported long back [38, 48-50]. Those reports showed that the increase of the transparent Al_2O_3 with a much smaller grain size of 1 μm could be obtained by a continuous hot-pressing process at 1400°C under pressures of 120 MPa in different atmosphere.

The major contribution to the less transparency for undoped polycrystalline Al_2O_3 originates from scattering caused by the remaining pores, and the difference between translucent and transparent Al_2O_3 could come entirely from the difference in pore-size and its distribution. Until quite recently, HIP is the most widely used technique for developing transparent alumina as it eliminates residual porosity and prevents grain growth leading to high transmission. For post-HIP treated samples, results for undoped [52], single doped (Mg^{2+}, Ti^{4+}) [39, 45, 46] transparent polycrystalline Al_2O_3 have been reported so far. This method gave fairly reproducible in-line transmittance between different groups with values up to 65 %.

Recently, some new sintering techniques such as microwave sintering [65] have also been studied for transparent crystalline Al_2O_3. Pressure-sintering such as HP and HIP is usually expensive in process cost. Microwave sintering is expected to realize homogeneous heating of the whole of ceramic sample.

4. Transparent Polycrystalline Al_2O_3 Produced by using PECS

Many reports on PECS for sintering transparent Al_2O_3 have been published as well as other transparent polycrystalline oxides. As process technology for ceramic powder is progressed, oxide ceramic powders with fine grain size and less agglomeration have been developed. Transparent polycrystalline Al_2O_3 with fine grains have been able to be prepared with such advanced oxide powder by using PECS.

Recently transparent oxide ceramics with fine grains such as 300 nm have been reported with different the PECS techniques as well as Al_2O_3. Munir and his colleagues promote PECS with ultra-high pressure such as 500 MPa [82]. High-pressure PECS is effective for preparing highly transparent polycrystalline Al_2O_3 [83], and also Y_2O_3-doped ZrO_2 [82] and Y_2O_3 [84]. High-pressure PECS is very useful for eliminate closed pores. However sample size is likely limited in high-pressure PECS.

Kim et al. proposed slow-heating PECS for densifying Al_2O_3 with less grain growth [57]. PECS with slow healing rate is available for not only Al_2O_3 but also $MgAl_2O_4$ [85]. Kim studied kinetics of densification and grain growth with stress rate in the point of view on “dynamic grain growth” [86]. He mentioned that slow stress rate in PECS is preferred in order to densification of Al_2O_3 with less grain growth. On the other hand, Makino and his colleagues reported that transparent polycrystalline Al_2O_3 can successfully obtained by PECS with fast heating rate such as 200 K/min [73]. However transparency of the sample with fast heating rate was not good in homogeneity. In order to densify Al_2O_3 without significant grain growth, influences of heating rate is still in discussion.

Goto and his colleagues reported PECS of transparent Lu_2O_3 with two-step pressure profile [87]. Lu_2O_3 is one of the candidates on laser host materials for high-power and ultra-short pulse lasers. However it is difficult for densification by conventional sintering. Taking account of advanced studies on transparent oxides given by Kim and Goto, a sintering profile is very important even in a process of PECS.

Thus PECS provides transparent polycrystalline oxides. Besides the oxides described here, there are many examples of transparent oxides sintered by using PECS. Table 1 shows a variety of transparent polycrystalline oxides prepared by using PECS.

Materials	Dopants	Remarks	Ref.
Al_2O_3	As-received	Slow-heating	[57]
	Cr_2O_3-doped		[76]
	As-received	High-pressure	[88]
	MgO, Y_2O_3 and La_2O_3-doped		[56]
	Cr_2O_3-doped	Slow-heating	[77]
	ZrO_2, La_2O_3 and MgO- doping		[78]
	MgO-doped	High-pressure	[83]
	As-received	Fast-heating	[73]
	As-received	Slow-heating	[80]
	La_2O_3-Doped	High-pressure	[81]
	As-received	Two-step temperature	[74, 75]
$MgAl_2O_4$	Undoped & LiF-doped	Two-step Pressure & Temperature	[89]
	As-received	Slow-heating	[85]
	As-received		[90]
	As-received		[91]
	As-received	Slow-heating	[92]
	Lab-made		[93]
Y_2O_3-Doped ZrO_2	As-received	High-pressure	[82]
	As-received		[94]
	As-received		[95]
	Lab-made		[96]
Y_2O_3	As-received, undoped	High-pssure	[97]

Materials	Dopants	Remarks	Ref.
	As-received, undoped		[98]
Lu_2O_3	As-received, undoped		[99]
	As-received, undoped	Two-step Pressure	[87]
	Lab-made, Yb_2O_3-doped		[100]
MgO	As-received		[101]
	Lab-made, Undoped & CaO-doped	High-pressure	[102]
$Lu_2Ti_2O_7$	Lab-made, undoped	Two-step Pressure	[103]
Lu_3NdO_7	Lab-made, undoped	Two-step Pressure	[104]
$La_2Zr_2O_7$	Lab-made, undoped	Two-step Pressure	[105]
β-$Ca_3(PO_4)_2$	undoped		[106]
YAG	undoped		[107]
	undoped &LiF-doped		[108]
	Lab-made, undoped		[109]
Oxyapatite	Lab-made, undoped		[110]
	Lab-made, undoped	High-pssure	[111]
Mullite	Lab-made, undoped		[112]

Table 1. Transparent polycrystalline oxides produced by PECS

5. Two-step PECS for transparent polycrystalline alumina

The authors study PECS with two-step temperature profile, that is, two-step PECS (referred as to TS-PECS), in order to fabricate transparent oxide ceramics with fine grains [74, 75]. Figure 3 shows the sintering profile of TS-PECS with other PECS techniques. TS-PECS can provide well-transparent oxides with shorter sintering period in comparison with slow-heating PECS.

Figure 4 shows appearance, fracture surface and density of polycrystalline Al_2O_3 prepared by using TS-PECS with 1st different temperature for 60 min and 1200°C for 20 min under 100 MPa in vacuum. A sample prepared by slow-heating PECS at 1200°C is shown for comparison. Importance of the 1st step temperature can be understood in Figure 4. The sample sintered at 1000°C in the 1st step has high transparency and less grain growth. The meaning of the 1st step is densification without significant grain growth. Sintering at 1000°C can provide densification without grain growth, however, full densification cannot be achieved. In order to reach to the full densification of the sample, the 2nd step with higher sintering temperature is necessary.

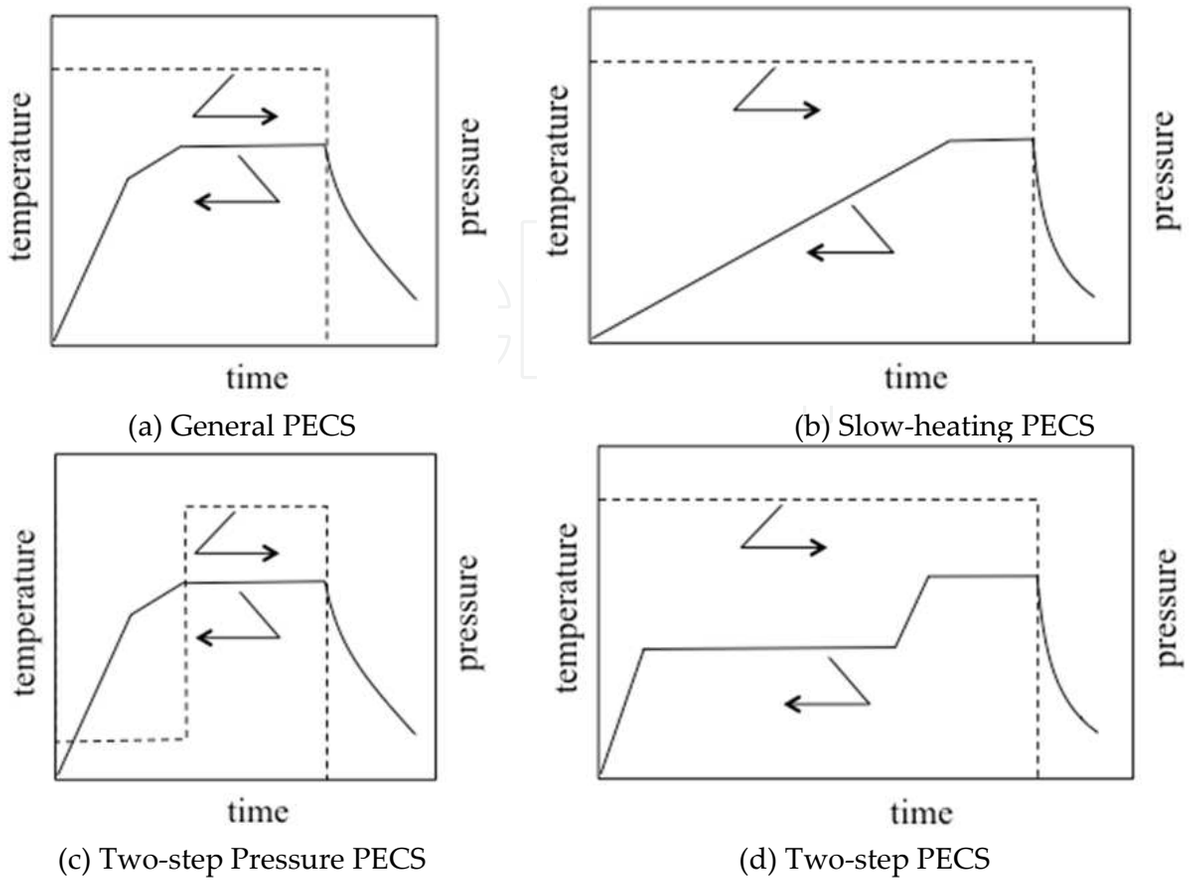

Figure 3. Schematic diagrams on sintering profiles of TS-PECS with other PECS techniques.

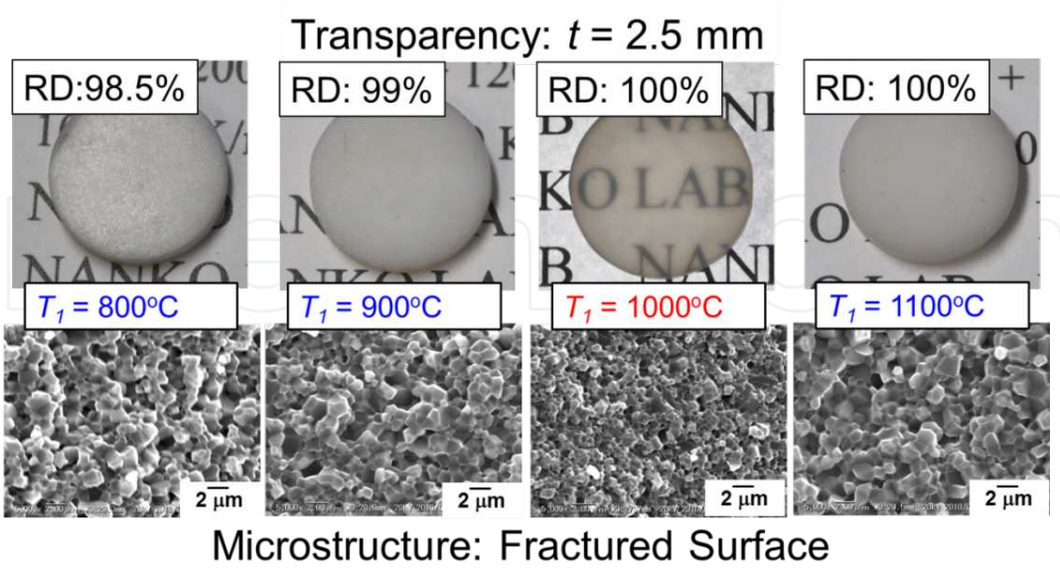

Figure 4. Appearance, fracture surface and density of polycrystalline Al_2O_3 prepared by using TS-PECS with 1st different temperature for 60 min and 1200°C for 20 min under 100 MPa in vacuum.

TS-PECS is also useful for other transparent oxides such as $MgAl_2O_4$. This polycrystalline oxide has better transparency because of isotropic crystal structure. Figure 5 shows appearance of polycrystalline $MgAl_2O_4$ produced by using TS-PECS. Even regular PECS such as 1300°C for 20 min with 100 K /min can provide transparent $MgAl_2O_4$ with fine grain size. However TS-PECS can increase transparency of the sintered sample.

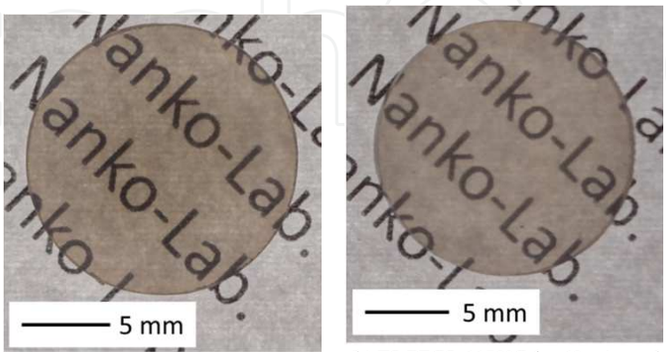

(a) PECS: 1300°C for 20 min

(b) TS-PECS: 1150°C for 60 min and 1350°C for 20 min

Figure 5. Appearance of polycrystalline $MgAl_2O_4$ produced by using (a) PECS and (b) TS-PECS under 100 MPa in vacuum.

Table 2 shows mechanical properties of transparent Al_2O_3 of TS-PECS. Bending strength of the samples is approximately 400 MPa, which is comparable with any commercial opaque Al_2O_3. This is caused by the existence of macroscopic defects as large as a few tens micrometers. Figure 6 shows an optical microscopic image of the inside of the transparent Al_2O_3 prepared by TS-PECS. Many black dots are observed in the sample. Figure 7 represents a scanning electron microscopic image of the cross-section of a black dot in transparent Al_2O_3 prepared by TS-PECS. Size of the black dot in Al_2O_3 is approximately 50 μm in diameter. The black dot is pores although the surrounding is fully densified. The microstructure of the black dots implies that the black dots were derived from the agglomeration of the initial particles of the Al_2O_3 powder. Such a larger defect leads low mechanical strength, as given by the Griffith Criteria. Even PECS with high pressure, the powder properties such as the agglomeration is very important. PECS under 100 MPa in uniaxial pressure cannot eliminate the agglomeration of the initial particles. In particular elimination of the agglomeration of the initial particles is very important in even PECS for structural ceramics and transparent ceramics.

Density	99.8%
Average Grain Size	0.31 μm
Vickers Hardness	20.8 GPa
Bending Strength	400 MPa
Fracture Toughness	3.3 $MPam^{1/2}$

Table 2. Mechanical Properties of Transparent Al_2O_3 prepared by TS-PECS (1000°C for 60 min, 1200°C for 20 min, 100MPa 100 K/min)

Figure 6 An optical microscopic image of the inside of the transparent Al_2O_3 prepared by TS-PECS

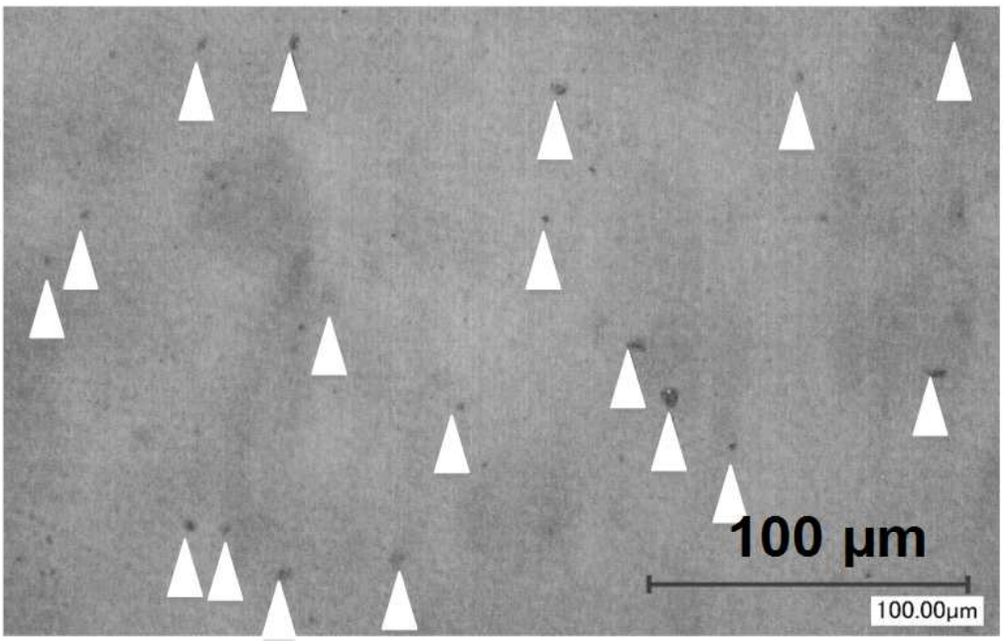

Figure 6. An optical microscopic image of the inside of the transparent Al_2O_3 prepared by TS-PECS

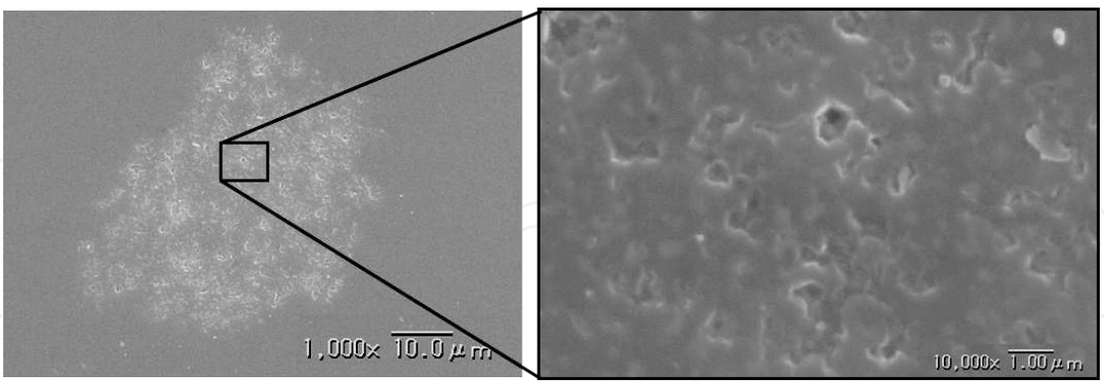

Figure 7. A scanning electron microscopic image of the cross-section of a black dot in transparent Al_2O_3.

TS-PECS is also available for preparing transparent colored-Al_2O_3 and $MgAl_2O_4$. Figure 7 shows appearance of various transparent Al_2O_3 and $MgAl_2O_4$ added with different dopants. A red color in Al_2O_3 and $MgAl_2O_4$ is caused by doping Cr_2O_3. In polycrystalline Al_2O_3, MnO causes the colour of orange or brown, however less transparency. Doping MnO into $MgAl_2O_4$ shows yellow in color and good transparency.

http://dx.doi.org/10.5772/59170

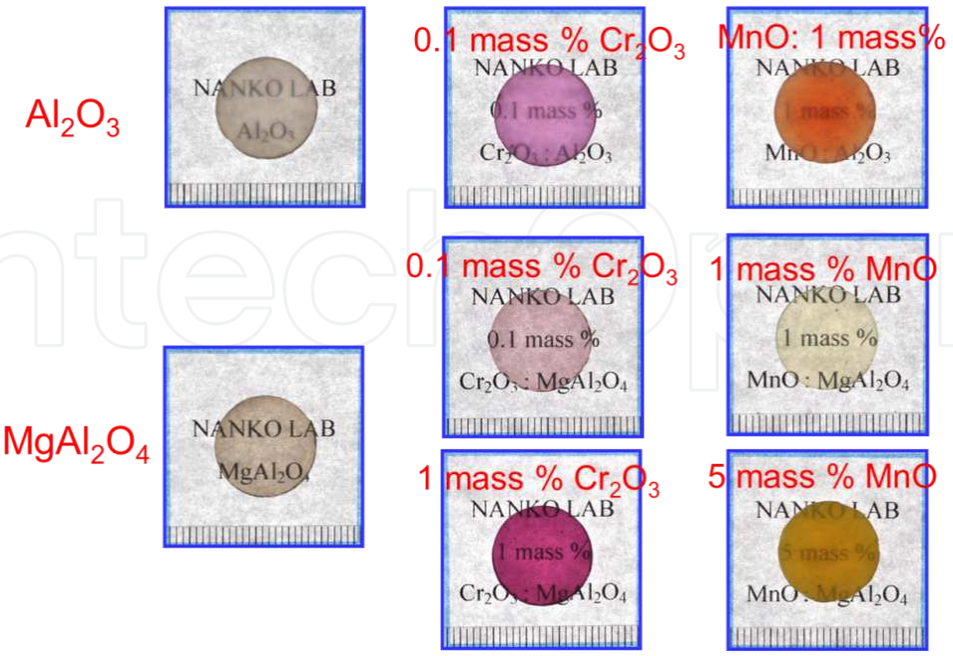

Figure 8. Appearance of various transparent Al_2O_3 and $MgAl_2O_4$ added with different dopants.

6. Summary

Transparent Polycrystalline Al_2O_3 can be produced by using PECS with advanced Al_2O_3 powder. The preferred techniques of PECS to obtain better transparency in Al_2O_3 are classified into the following: (1) high-pressure PECS, (2) slow-heating PECS, (3) fast-heating PECS, and (4) two-step PECS, as well as PECS with preferred additives. Influences in sintering parameters in PECS for transparent polycrystalline Al_2O_3 are still not clear. At least, PECS with slow heating rate and two-step heating profile is preferred to produce transparent polycrystalline Al_2O_3. Using advanced Al_2O_3 powder and PECS, agglomeration of the particles is still significant issue in transparent polycrystalline Al_2O_3. Management of Al_2O_3 powder to reduce the agglomeration is necessary to increase transparency of Al_2O_3 prepare by using PECS.

Acknowledgements

The authors thank to Mr. Masakazu Kawahara (Fuji Electric Industry Co. Ltd.) and Mr. Shinichi Takei (SinterLand Inc.) for useful discussion and Mr. Huu Hien Nguyen who is a graduate student of Nagaoka University of Technology, for conducting experiments on colored Al_2O_3 and $MgAl_2O_4$ and observation of black dots in transparent polycrystalline Al_2O_3.

Author details

Makoto Nanko[1*] and Khanh Quoc Dang[2]

*Address all correspondence to: nanko@mech.nagaokaut.ac.jp

1 Department of Mechanical Engineering, Nagaoka University of Technology, Japan

2 School of Materials Science and Engineering, Hanoi University of Science and Technology, Vietnam

References

[1] Shevell SK. The science of color. Elsevier, Oxford, UK; 2003.

[2] Grasso S., Sakka Y., Maizza G. Electric Current Active/assisted Sintering (ECAS): a Review of Patents 1906-2008. Science and Technology of Advanced Materials 2009; 10 053001/1-24.

[3] Munir ZA., Anselmi-Tamburini U., Oyanagi M. The Effect of Electric Field and Pressure on the Synthesis and Consolidation of Materials: A Review of the Spark Plasma Sintering Method. Journal of Materials Science 2006; 41 763-777.

[4] Duval D'Adrian AL. Article of Fused Metallic Oxide and Process of Producing the Same. US Patent No. 1,430,724 1922.

[5] Bloxam AG. Improved Manufacture of Electric Incandescence Lamp Filaments from Tungsten or Molybdenum or an Alloy Thereof. GB Patent No. 190527002 1906.

[6] Bloxam AG. Improved Manufacture of Filaments of Tungsten or Molybdenum for Electric Incandescence Lamps. GB Patent No. 190609020 1906.

[7] Taylor GF. Improvements in and Relating to Methods of and Apparatus for Producing Hard Metal Compositions. GB Patent No. 385629 1932.

[8] Taylor GF. Apparatus for Making Hard Metal Compositions. US Patent No. 1896854 1933.

[9] Taylor GF. Welding Process. US Patent No. 1896853 1933.

[10] Kim DK., Pak HR., Okazaki K. Electrodischarge Compaction of Nickel Powders. Materials Science and Engineering A 1988; 104 191-200.

[11] Inoue K. Electric-Discharge Sintering. US Patent No. 3241956 1966.

[12] Inoue K. Apparatus for Electrically Sintering Discrete Bodies. US Patent No. 3250892 1966.

[13] Yoo SH., Sethuram KM., Sudarshan TS. Apparatus for Bonding a Particle Material to Near Theoretical Density. US Patent No. 5989487 1999

[14] Tokita M. Trends in Advanced SPS Spark Plasma Sintering Systems and Technology. Journal of the Society of Powder Technology, Japan 1993; 30 790-804.

[15] Inoue K. Method and Apparatus for Electric Discharge Sintering. JP Patent No. 03056604 1991.

[16] Orrù R., Richeri R., Locci AM., Cincotti A., Cao G. Consolidation/synthesis of Materials by Electric Current Activated/assisted Sintering. Materials Science and Engineering R 2009; 63 127-287.

[17] Mirva E. Spark plasma sintering and deformation bihaviour of Titanium and Titanium/TiB2 composites. Licentiate thesis. Stockholm University; 2007.

[18] Matsugi K., Kuramoto H., Hatayama T., Yanagisawa O. Temperature distribution at steady state under constant current discharge in spark sintering process of Ti and Al_2O_3 powders. Journal of Materials Processing Technology 2003; 134 225-232.

[19] Wang YC., Fu ZY., Wang WM., Zhu HX. Temperature Field Distribution in Spark Plasma Sintering of BN. ournal of Wuhan University of Technology 2002; 17 19-21.

[20] Nanko M., Maruyama T., Tomino H. Neck Growth on Initial Stage of Pulse Current Pressure Sintering for Coarse Atomized Powder Made of Cast-iron. Journal of the Japan Institute of Metals 1999; 63 917-923.

[21] Nanko M., Oyaidu T., Maruyama T. Densification of Ni-20Cr alloy course-powder by pulse current pressure sintering. Journal of the Japan Institute of Metals 2002; 66 87-93.

[22] Kim HT., Kawahara M., Tokita M. Specimen temperature and sinterability of Ni powder by spark plasma sintering. Journal of the Japan Society of Powder and Powder Metallurgy 2000; 47(8) 887-891

[23] Wang Y., Fu Z., Zhang Q. SPS Temperature Distribution of Different Conductivity Materials. Key Engineering Materials 2002; 224-226 717-720

[24] Tomino H., Watanabe H., Kondo Y. Electric Current Path and Temperature Distribution for Spark Sintering. Journal of the Japan Society of Powder and Powder Metallurgy 1997; 44 974-979.

[25] Xie G., Ohashi O., Chiba K., Yamaguchi N., Song M., Furuya K., Noda T. Frequency Effect on Pulse Electric Current Sintering Process of Pure Aluminum Powder. Materials Science and Engineering A 2003; 359 384-390.

[26] Chen W., Anselmi-Tamburini U., Garay JE., Groza JR., Munir ZA. Fundamental Investigation on the Spark Plasma Sintering/ Synthesis Process I. Effect of DC Pulsing on Reactivity. Materials Science and Engineering A 2005; 394 132-138.

[27] Anselmi-Tamburini U., Garay JE., Munir ZA. Fundamental Investigations on the Spark Plasma Sintering/ Synthesis Process III. Current Effect on Reactivity", Materials Science and Engineering A 2005; 407 24-30.

[28] Kondo T., Yasuhara M., Kuramoto T., Kodera Y., Ohyanagi M., Munir ZA. Effect of Pulsed DC Current on Atomic Diffusion of Nb-C Diffusion Couple. Journal of Materials Science 2008; 43 6400-6405.

[29] Kondo T., Kuramoto T., Kodera Y., Ohyanagi M., Munir ZA. Influence of Pulsed DC Current and Electric Field on Growth of Carbide Ceramics during Spark Plasma Sintering. Journal of the Ceramic Society of Japan 2008; 116 1187-1192.

[30] Kondo T., Kuramoto T., Kodera Y., Ohyanagi M., Munir ZA. Enhanced Growth of Mo_2C Formed in Mo-C Diffusion Couple by Pulse DC Current. Journal of the Japan Society of Powder and Powder Metallurgy2008; 55 643-650.

[31] Inoue K. Electric Discharge Heat Treatment of Metals in Electrolytes. US Patent No. 3,188,245; 1965.

[32] Nishimoto K., Saida KJ., Tsuzuki R. Effect of Pulsed Electric-current on Densification Behavior of Bonded Interlayer of Oxide-dispersion-strengthened Super Alloys Joint. Journal of the Japan Institute of Metals 2001; 65(8) 747-755.

[33] Dang QK., Nanko M., Kawahara M., Takei S. Densification of Alumina Powder by Using PECS Process with Different Pulse Electric Current Waveforms. Materials Science Forum 2009; 620-622 101-104.

[34] Dang QK., Nanko N. Effects of ON/OFF Pulse pattern on Sintering Alumina by a Pulsed Electric Current Sintering Process. Journal of Ceramic Processing Research 2009; 10 s32-s38.

[35] Dang QK., Kawahara M., Takei S., Nanko M. Effects of Pulsed Current Waveforms on Sample Temperature and Sintering Behavior in PECS of Alumina. Journal of the Japan Society of Powder and Powder Metallurgy 2009; 56 780-787.

[36] Anselmi-Tamburini U., Gennari S., Garay JE., Munir ZA. Fundamental Investigations on the Spark Plasma Sintering/ Synthesis Process II. Modeling of Current and Temperature Distributions. Materials Science and Engineering A 2005; 394 139-148.

[37] Zhang DM., Fu ZY., Wang YC., Zhang QJ., Guo JK. Heterogeneous of Non-conductive Materials Sintering by Pulse Electric Current. Key Engineering Materials 2002; 224-226 729-734.

[38] Peelen JGJ., Metselaar R. Light Scattering by Pores in Polycrystalline Materials: Transmission Properties of Alumina. Journal of Applied Physics 1974; 45 216-220.

[39] Apetz R., Bruggen MPB. Transparent Alumina: a Light-scattering Model. Journal of the American Ceramic Society 2003; 86 480-486.

[40] Pecharromàn C., Mata-Osoro G., Antonio Dìaz L., Torrecillas R., Moya JS. On the transparency of nanostructured alumina: Rayleigh-Gans Model for Anisotropic Spheres. Optics Express 2009; 17 6899-6912.

[41] Mizuta H., Oda K., Shibasaki Y., Maeda M., Machida M., Ohshima K. Preparation of High-Strength and Translucent Alumina by Hot Iso-Static Pressing. Journal of the American Ceramic Society 1992; 75 469-73.

[42] Coble RL. Transparent Alumina and Method of Preparation. U.S. Patent No. 3,026,210 1962.

[43] Wei GC., Rhodes WH. Sintering of Translucent Alumina in a Nitrogen–Hydrogen Gas Atmosphere. Journal of the American Ceramic Society 2000; 83 1641-8.

[44] Mao XJ., Wang SW., Shimai S., Guo JK. Transparent Polycrystalline Alumina Ceramics with Orientated Optical Axes. Journal of the American Ceramic Society 2008; 91 3431-3.

[45] Krell A., Blank P., H. Ma, Hutzler T. Transparent Sintered Corundum with High Hardness and Strength. Journal of the American Ceramic Society 2003; 86 12-18.

[46] Bernard-Granger G., Guizard C. Influence of MgO or TiO2 Doping on the Sintering Path and on the Optical Properties of a Submicronic Alumina Material. Scripta Materialia 2007; 56 983-986.

[47] Kim DS., Lee JH., Sung RJ., Kim SW., Kim HS., Park JS. Improvement of Translucency in Al_2O_3 Ceramics by Two-step Sintering Technique. Journal of the European Ceramic Society 2007; 27 3629-3632.

[48] Peelen JGJ., Metselaar R. Light Scattering by Pores in Polycrystalline Materials: Transmission Properties of Alumina. Journal of Applied Physics 1974; 45 216-220.

[49] Peelen JGJ. Light Transmission of Sintered Alumina. Philips Technical Review 1976; 36 47-52.

[50] Peelen JGJ. Transparent Hot-pressed Alumina. I: Hot Pressing of Alumina. Ceramurgia International 1979; 5 70-75.

[51] Peelen JGJ. Transparent Hot-pressed Alumina. II: Transparent versus Translucent Alumina. Ceramurgia International 1979; 5 115-119.

[52] Krell A., Klimke J., Hutzler T. Advanced Spinel and Sub-μm Al_2O_3 for Transparent Armour Applications. Journal of the European Ceramic Society 2009; 29 275-281.

[53] Jiang D., Hulbert DM., Anselmi-Tamburini U., Ng T., Land D., Mukherjee AK. Optically Transparent Polycrystalline Al_2O_3 Produced by Spark Plasma Sintering. Journal of the American Ceramic Society 2008; 91 151-154.

[54] Aman Y., Garnier V., Djurado E. Influence of Green State Processes on the Sintering Behaviour and the Subsequent Optical Properties of Spark Plasma Sintered Alumina. Journal of the European Ceramic Society 2009; 29 3363-3370.

[55] Suárez M., Fernández A., Menéndez J.L., Torrecillas R. Grain Growth Control and Transparency in Spark Plasma Sintered Self-doped Alumina Materials. Scripta Materialia 2009; 61 931-934.

[56] Stuer M., Zhao Z., Aschauer U., Bowen P. Transparent Polycrystalline Alumina Using Spark Plasma Sintering: Effect of Mg, Y and La doping. Journal of the European Ceramic Society 2010; 30 1335-1343.

[57] Kim BN., Hiraga K., Morita K., Yoshida H. Spark Plasma Sintering of Transparent Alumina. Scripta Materialia 2007; 57 607-610.

[58] Kim BN., Hiraga K., Morita K., Yoshida H. Effects of Heating Rate on Microstructure and Transparency of Spark Plasma Sintered Alumina. Journal of the European Ceramic Society 2009; 29 323-327.

[59] Kim BN., Hiraga K., Morita K., Yoshida H., Miyazaki T., Kagawa Y. Microstructure and Optical Properties of Transparent Alumina. Acta Materialia 2009; 57 1319-1326.

[60] O YT., Koo J., Hong KJ., Park JS., Shin DC. Effect of Grain Size on Transmittance and Mechanical Strength of Sintered Alumina. Materials Science and Engineering A 2004; 374 191-195.

[61] Pecharromàn C., Mata-Osoro G., Antonio Dìaz L., Torrecillas R., Moya JS. On the transparency of nanostructured alumina: Rayleigh-Gans Model for Anisotropic Spheres. Optics Express 2009; 17 6899-6912.

[62] Braun A., Falk G., Clasen R. Transparent Polycrystalline Alumina Ceramic with Submicrometre Microstructure by Means of Electrophoretic Deposition. Material Wissenschaft und Werkstofftechnik 2006; 37 293-297.

[63] Krell A., Blank P., Ma H., Hutzler T. and Nebelung M. Processing of High-Density Submicrometer Al_2O_3 for New Applications. Journal of the American Ceramic Society 2003; 86 546-553.

[64] Krell A., Klimke J. Effects of the Homogeneity of Particle Coordination on Solid-state Sintering of Transparent Alumina. Journal of the American Ceramic Society 2006; 89 1985-1992.

[65] Krell A., Blank P. Grain size Dependence of Hardness in Dense Submicrometer Alumina. Journal of the American Ceramic Society 1995; 78 (4) 1118-1120.

[66] Cheng J., Agarwal D., Zhang Y., Roy R. Microwave Sintering of Transparent Alumina. Materials Letters 2002; 56(4) 587-592.

[67] Kwon OH., Nordahl CS., Messing GL. Submicrometer Transparent Alumina by Sinterforging Seeded γ-alumina Powders. Journal of the American Ceramic Society 1995; 78 491-494.

[68] Grasso S., Kim BN., Hu C., Maizza G., Sakka Y. Highly Transparent Pure Alumina Fabricated by High-pressure Spark Plasma Sintering. Journal of the American Ceramic Society 2010; 93 2460-2462.

[69] Hayashi K., Kobayashi O., Toyoda S., Morinaga K. Transmission Optical Properties of Polycrystalline Alumina with Submicron Grains. Materials Transactions, JIM 1991; 32 1024-1029.

[70] Aman Y., Garnier V., Djurado E. A Screening Design Approach for the Understanding of Spark Plasma Sintering Parameter: A Case of Translucent polycrystalline Undoped Alumina. International Journal of Applied Ceramic Technology 2010; 7 574-586.

[71] Chakravarty D., Bysakh S., Muraleedharan K., Rao T.N., Sundaresan R. Spark Plasma Sintering of Magnesia-doped Alumina with High Hardness and Fracture Toughness. Journal of the American Ceramic Society 2008; 91 203-208.

[72] Park CW., Yoon DY. Effects of SiO2, CaO2, and MgO additions on the Grain Growth of Alumina. Journal of the American Ceramic Society 2000; 83 2605-609.

[73] Dobedoe RS., West GD., Lewis MH. Spark Plasma Sintering of Ceramics. Bulletin of the European Ceramic Society 2003; 1 19-24.

[74] Makino Y, Kawahara M, Sakaguchi M, Kaiyama Y, Akatsuka K, Yasuno T, J. Jpn. Powder Powder Metall., 2012; 59 (9) 532-537.

[75] Dang K. Q, Nanko M, transparent alumina prepared by two-step sintering in pulsed electric current sintering. in PM2012: proceedings of PM2012, 14-18 October 2012, Yokohama, Japan; 2013.

[76] Nanko M, Dang K. Q., Two-step Pulsed Electric Current Sintering of Transparent Al_2O_3 Ceramics, Adv. Appl. Ceram.2014; 113 (2) 80-84.

[77] Wang C, Zhao Z, Transparent Polycrystalline Ruby Ceramic by Spark Plasma Sintering, Mater. Res. Bull. 2010; 45 (9) 1127-1131.

[78] Dang K. Q., Kawahara M, Takei S, Nanko M, Fabrication of Transparent Cr-Doped Al2O3 Made by Pulsed Electric Current Sintering Process, Ceram. Intl. 2011; 37 957-963.

[79] Roussel N, Lallemant L, Durand B, Guillemet S, Chane Ching J.-Y., Fantozzi G, Garnier V, Bonnefont G, Effects of the Nature of the Doping Salt and of the Thermal Pretreatment and Sintering Temperature on Spark Plasma Sintering of Transparent Alumina, Ceram. Intl. 2011; 37 (8) 3565-3573.

[80] Kim B.N., Hiraga K, Grasso S, Morita K, Yoshida H, Zhang H, Sakka Y, High-pressure Spark Plasma Sintering of MgO-doped Transparent Alumina, J. Ceram. Soc. Jpn. 2012; 120 (3) 116-118.

[81] Lallemant L,Fantozzi G, Garnier V, Bonnefont G, Transparent Polycrystalline Alumina Obtained by SPS: Green Bodies Processing Effect, J. Euro. Ceram. Soc. 2012; 32 2909-2915.

[82] Roussel N, Lallemant L, Chane-Ching J.-Y., Guillemet-Fristch S, Durand B, Garnier V, Bonnefont G, Fantozzi G, Bonneau L, Trombert S, Garcia-Gutierrez D, Highly Dense, Transparent α-Al_2O_3 Ceramics From Ultrafine Nanoparticles Via a Standard SPS Sintering, J. Amer. Ceram. Soc., 2013; 96 (4) 1039-1042.

[83] Anselmi-Tamburini U, Garay J.E., Munir Z.A., Fast Low-temperature Consolidation of Bulk Nanometric Ceramic Materials, Scripta Mater. 2006; 54 823-828.

[84] Kim B.N., Hiraga K, Grasso S, Morita K, Yoshida H, Zhang H, Sakka Y, High-pressure Spark Plasma Sintering of MgO-doped Transparent Alumina, J. Ceram. Soc. Jpn. 2012; 120 (3) 116-118.

[85] Zhang H, Kim B.-N. Morita K, Yoshida H, Hiraga K, Sakka Y, Fabrication of Transparent Yttria by High-Pressure Spark Plasma Sintering, J. Amer. Ceram. Soc., 2011; 94 (10) 3206–3210.

[86] Morita K, Kim B.N., Hiraga K, Yoshida H, Fabrication of transparent $MgAl_2O_4$ Spinel polycrystal by spark plasma sintering processing, Scripta Mater.2008; 58, 1114-1117.

[87] Kim B.N., Hiraga K, Morita K, Yoshida H, Park Y. J., Sakka Y, Dynamic Grain Growth during Low-temperatrue Spark Plasma Sintering of Alumina, Scripta Mater. 2014; 80() 29-32.

[88] An L, Ito A, Goto T, Two-step Pressure Sintering of Transparent Lutetium Oxide by Spark Plasma Sintering, J. Euro Ceram. Soc.2011; 31 1597–1602.

[89] Gasso S, Kim B. N., Hu C, Mizza G, Sakka Y, Highly Transparent Pure Alumina Fabricated by High-Pressure Spark Plasma Sintering. J. Amer. Ceram. Soc. 2010; 93 (9) 2460-24 62.

[90] Frage N, Cohen S, Meir S, Kalabukhov S, Dariel M. P., Spark Plasma Sintering (SPS) of Transparent Magnesium-aluminate Spinel, J. Mater. Sci. 2007; 42 3273-3275.

[91] Bernard-Granger G, Benameur N, Guizard C, Nygren M, Influence of Graphite Contamination on the Optical Properties of Transparent Spinel Obtained by Spark Plasma Sintering, Script Mater. 1009; 60 164-167.

[92] Wang C, Zhao Z, Transparent $MgAl_2O_4$ Ceramic Produced by Spark Plasma Sintering, Scripta Mater.2009; 61 (2), 193-196.

[93] Bonnefonta G, Fantozzi G, Trombert S, Bonneau L, Fine-grained Transparent $MgAl_2O_4$ Spinel Obtained by Spark Plasma Sintering of Commercially Available Nanopowders, Ceram. Intl. 2012; 38 (1) 131-140.

[94] Fu P, Lu W, Lei W, Xu Y, Wang X, Wu J, Transparent Polycrystalline $MgAl_2O_4$ Ceramic Fabricated by Spark Plasma Sintering: Microwave Dielectric and Optical Properties, Ceram. Intl. 2013: 39 (3) 2481-2487.

[95] Casolco S. R., Xu J, Garay J. E., Transparent/translucent Polycrystalline Nanostructured Yttria Stabilized Zirconia with Varying Colors, Scripta Mater. 2008; 58, 516-519.

[96] Alaniz J. E., Perez-Gutierrez F. G., Aguilar G, Garay J. E., Optical Properties of Transparent Nanocrystalline Yttria Stabilized Zirconia, Opt. Mater. 2009; 32 62–68.

[97] Lei L.W., Fu Z.Y., Wang H, Lee S.W., Niihara K., Transparent Yttria Stabilized Zirconia from Glycine-nitrate Process by Spark Plasma Sintering, Ceram. Intl., 2012; 38 (1) 23-28.

[98] Zhang H, Kim B.-N. Morita K, Yoshida H, Hiraga K, Sakka Y, Fabrication of Transparent Yttria by High-Pressure Spark Plasma Sintering, J. Amer. Ceram. Soc., 2011; 94 (10) 3206–3210.

[99] An L, Ito A, Goto T, Transparent Yttria Produced by Spark Plasma Sintering at Moderate Temperature and Pressure Profiles, J. Euro. Ceram. Soc. 2012; 32 (5) 1035–1040.

[100] An L, Ito A, Goto T, Fabrication of Transparent Lutetium Oxide by Spark Plasma Sintering, J. Amer. Ceram. Soc. 2011; 94 (3) 695-698.

[101] Prakasam M, Viraphong O, Michau D, Veber P, Velázquez M, Shimamura K, Largeteau A, Yb^{3+} Doped Lu_2O_3 Transparent Ceramics by Spark Plasma Sintering, Ceram. Intl. 2013; 39 1307-1313.

[102] Chaim R, Shen Z, Nygren M, Transparent Nanocrystalline MgO by Rapid and Low-temperature Spark Plasma Sintering, J. Mater. Res. 2004; 19 (4) 2527-2531.

[103] Tran T. B., Hayun S, Navrotsky A, Castro R. H. R., Transparent Nanocrystalline Pure and Ca-Doped MgO by Spark Plasma Sintering of Anhydrous Nanoparticles, J. Amer. Ceram. Soc. 2012; 95 (4) 1185-1188.

[104] An L, Ito A, Goto T, Highly Transparent Lutetium Titanium Oxide Produced by Spark Plasma Sintering, J. Euro. Ceram. Soc. 2011; 31 237-240.

[105] An L, Ito A, Goto T, Fabrication of Transparent Lu_3NbO_7 by Spark Plasma Sintering, Mater. Lett. 2011; 65 3167-3169.

[106] An L, Ito A, Goto T, Fabrication of Transparent $La_2Zr_2O_7$ by Reactive Spark Plasma Sintering, Key Eng. Mater. 2011; 484 135-138.

[107] Kawagoe D, Ioku K, Fujimori H, Goto S, Transparent β-Tricalcium Phosphate Ceramics Prepared by Spark Plasma Sintering, J. Ceram. Soc. Jpn. 2004; 112 (8) 462-463.

[108] Chaim R, Marder-Jaeckel R., Shen J. Z., Transparent YAG Ceramics by Surface Softening of Nanoparticles in Spark Plasma Sintering, Mater. Sci. Eng. A 2006; 429 (1/2) 74-78.

[109] Frage N, Kalabukhov S, Sverdlov N, Ezersky V, Dariel M. P., Densification of Transparent Yttrium Aluminum Garnet (YAG) by SPS Processing, J. Euro. Ceram. Soc. 2010; 30 3331-3337.

[110] Spina G, Bonnefont G, Palmero, Fantozzi G, Chevalier J, Montanaro L, Transparent YAG Obtained by Spark Plasma Sintering of Co-precipitated Powder. Influence of Dispersion Route and Sintering Parameters on Optical and Microstructural Characteristics, J. Euro. Ceram. Soc. 2012; 32 2957-2964.

[111] Chesnaud A, Bogicevic C, Karolak F, Estournes C, Dezanneau G, Preparation of Transparent Oxyapatite Ceramics by Combined Used of Freeze-drying and Spark-plasma Sintering, Chem. Commun. 2007 1550-1552.

[112] Eriksson M, Liu Y, Hu J, Gao L, Nygren M, Shen Z, Transparent hydroxyapatite Ceramics with Nanograin Structure Prepared by High Pressure Spark Plasma Sintering at the minimized Sintering Temperature, J. Euro. Ceram. Soc. 2011; 31 1533-1540.

[113] Zhang G, Wang Y, Fu Z, Wang H, Wang W, Zhang J, Lee S.-W., Niihara K, Transparent Mullite Ceramic from Single-Phase Gel by Spark Plasma Sintering, J. Euro. Ceram. Soc. 2009; 29 2705-2711.